

Copyright
by
Jaideep Shivaprasad Bhagmane
2009

**The Thesis Committee for Jaideep Shivaprasad Bhagmane
Certifies that this is the approved version of the following thesis:**

**Using Mortars to Upscale Permeability in Heterogeneous Porous Media
from the Pore to Continuum Scale**

**APPROVED BY
SUPERVISING COMMITTEE:**

Supervisor:

Matthew T Balhoff, Supervisor

David DiCarlo, Reader

**Using Mortars to Upscale Permeability in Heterogeneous Porous Media
from the Pore to Continuum Scale**

BY

Jaideep Shivaprasad Bhagmane, B.E.

Thesis

Presented to the Faculty of the Graduate School of

The University of Texas at Austin

in Partial Fulfillment

of the Requirements

for the Degree of

Master of Science in Engineering

The University of Texas at Austin

December 2009

DEDICATION

I would like to dedicate my thesis to my mother, HR Bhagyalakshmi for giving me all the love and support.

ACKNOWLEDGEMENTS

I would like to specially thank Dr. Matthew Balhoff for giving me the opportunity to work in his group. The supervision and guidance received has been vital and crucial, not only with regards to my thesis but my graduate program as a whole. Secondly, I would like to take this opportunity to thank Dr. David DiCarlo, for taking the time to review my thesis. I would also like to thank Chrissi King and Dr. Sunil Thomas for the invaluable assistance and the ideas suggested. My sincere acknowledgements to the Texas Advanced Computing Centre (TACC) and the personnel at TACC, for allowing me to run simulations and in providing round the clock assistance.

Rob, Greg, Tie, Ali, Hari, Abraham & Aviral as colleagues and friends have been vital in helping me overcoming research-obstacles. The countless discussions on topics ranging from pore-networks to soccer have been ever so intellectually stimulating, and beneficial towards the understanding and completion of my work. I would also like to thank Dr. Terzian for all the IT assistance and Dr. Masa for the weekly insights into pore-network behavior.

Last but not the least I would like to acknowledge my father, BK Shivaprasad, mother, HR Bhagyalakshmi, and brother, BS Bharat, for the constant and never-ending support. I would also like to thank all the others who in their unique ways have contributed towards me achieving my work.

December, 2009

ABSTRACT

Using Mortars to Upscale Permeability in Heterogeneous Porous Media from the Pore to Continuum Scale

Jaideep Shivaprasad Bhagmane, M.S.E.

The University of Texas at Austin, 2009

Supervisor: Matthew T. Balhoff

Pore-scale network modeling has become an effective method for accurate prediction and upscaling of macroscopic properties, such as permeability. Networks are either mapped directly from real media or stochastic methods are used that simulate their heterogeneous pore structure. Flow is then modeled by enforcing conservation of mass in each pore and approximations to the momentum equations are solved in the connecting throats. In many cases network modeling compares favorably to experimental measurements of permeability. However, computational and imaging restrictions generally limit the network size to the order of 1 mm^3 (few thousand pores). For extremely heterogeneous media these models are not large enough in capturing the petrophysical properties of the entire heterogeneous media and inaccurate results can be obtained when upscaling to the continuum scale. Moreover, the boundary conditions imposed are artificial; a pressure gradient is imposed in one dimension so the influence of flow behavior in the surrounding media is not included.

In this work we upscale permeability in large, heterogeneous media using physically-representative pore-scale network models (domain $\sim 10^6$ pores). High-performance computing is used to obtain accurate results in these models, but a more efficient, novel domain decomposition method is introduced for upscaling the permeability of pore-scale models. The medium is decomposed into hundreds of smaller networks (sub-domains) and then coupled with the surrounding models to determine accurate boundary conditions. Finite element mortars are used as a mathematical tool to ensure interfacial pressures and fluxes are matched at the interfaces of the networks boundaries. The results compare favorably to the more computationally intensive (and impractical) approach of upscaling the media as a single model. Moreover, the results are much more accurate than traditional hierarchical upscaling methods. This upscaling technique has important implications for using pore-scale models directly in reservoir simulators in a multiscale setting. The upscaling techniques introduced here on single phase flow can also be easily extended to other flow phenomena, such as multiphase and non-Newtonian behavior.

TABLE OF CONTENTS

List of Tables	x
List of Figures.....	xi
List of Figures.....	xi
Chapter 1: Summary	1
Chapter 2: Background	2
2.1 Introduction.....	2
2.2 Pore-Network Models.....	4
2.3 Representative Elementary Volume (REV).....	6
2.4 Boundary Conditions	7
2.5 Finite Element Method	8
2.5.1 Mortar Coupling.....	9
2.6 Finite Difference Method.....	10
2.7 Objective.....	11
Chapter 3: Network Generation and Solution.....	13
3.1 Model Generation	13
3.1.1 Medial Axis Algorithm	14
3.1.2 Maximum Ball Algorithm	14
3.1.3 Probabilistic Population.....	15
3.1.4 Detailed Description of Network Generation	19
3.2 Model Solution.....	20
3.3 Domain Decomposition (Dividing the Pore Network).....	21
3.4 Finite Difference	23
3.5 Finite Element Mortars	26
3.5.1 Coupling with Mortars.....	27
3.5.2 Coupling Example Using Linear Mortars.....	28

Chapter 4: Results/Discussion	33
4.1 Million Pore Large Network.....	33
4.2 Finite Difference Simulation.....	34
4.3 Mortar-Coupled Results.....	37
Chapter 5: Conclusion.....	42
Appendix A	44
Glossary	48
References.....	50
Vita	53

LIST OF TABLES

Table 1	Permeability comparisons between K_{true} , K_{mortar} and K_{FD} . Number of pores in network A is 1,000,088 pores and network B has 1,000,071. Probability distribution parameters are given in Table A.1.34	34
Table 2:	Pore network model simulation times, for 1,000,088 pores (network-A). Simulation times (K_{mortar}) can be further improved by parallel computing. Simulations have been run using one node of the 1300 node Lonestar Linux Cluster (TACC). A node consists of a Dell PowerEdge 1955 blade running a 2.6 x86_64 Linux kernel. Each node contains two Xeon Intel Duo-Core 64-bit processors on a single board, as an SMP unit. The core frequency is 2.66GHz and supports 4 floating-point operations per clock period with a peak performance of 10.6 GFLOPS/core or 42.6GFLOPS/node. Each node contains 8GB of memory41	41
Table A.1:	Network generation parameters (Refer eq. 1) Both network types (A and B) have the same parameter range. Network B is anisotropic than network A due to the distribution of high & low permeability networks into channels having high and low flow-regimes.44	44

LIST OF FIGURES

Figure 1:	Visual depiction of the REV for a porous media with porosity as the measured quantity.7	7
Figure 2:	Diagonally dominant, sparse symmetric matrix (A) resulting while utilizing the FEM method. Each point on the figure represents a data value.9	9
Figure 3:	Probability distributions (Berea) used in model generation (Venkatarangan 2000).....16	16
Figure 4:	The above figure illustrates the connection between $p(\text{rnd}_1)$ and $p(x_1)$ via the equation of $F(\text{rnd})$ equal $F(x)$. $p(\text{rnd}_1)$ and $p(x_1)$ are the probability distributions of the uniform and subject distribution and $F(\text{rnd})$ and $F(x)$ are the integrals of these probability distributions. (Steven Jacques, 1998)18	18
Figure 5:	Example large network divided into 5x5 sub-network grids (total pores = 4720, range = 70-400 pores)22	22
Figure 6:	Plot showing the permeabilities of the 10x10 sub-networks, (a) Network A (b) Network B. In each block, the values on the top are the permeabilities for the K_{xx} configuration and values at the bottom are the permeabilities for the K_{yy} configuration.24	24
Figure 6:	(continued) Plot showing the permeabilities of the 10x10 sub-networks, (a) Network A (b) Network B. In each block, the values on the top are the permeabilities for the K_{xx} configuration and values at the bottom are the permeabilities for the K_{yy} configuration.....25	25

Figure 7(a): Illustration of two sub-networks (sub-network 1&2) showing their interface boundary with example boundary pores BP1 and BP2 on sub-network 1&2 respectively. The interconnecting mortar mesh (1x1 linear mortar) is also shown in between the sub-networks. Note the X and Y axis.	31
Figure 7(b): Illustration of the 1x1 mortar mesh, note the alphas ($\alpha_1, \alpha_2, \alpha_3, \alpha_4$) at the four corners and also geometrical depiction of the basis functions in grey shading.	31
Figure 8: Flow chart showing mortar coupling logic.	32
Figure 9: Contour plots of (a) network A and (b) network B showing the pressure variations for the finite difference solution. The parameters in colored boxes are pressures.	36
Figure 10(a): Contour plot of the true interface pressure solution.	39
Figure 10(b): Contour Plots of the K_{mortar} solutions. Pressure solution taken from the interface between the 3(row) X 5(column) sub-network and the 3(row) X 6(column) sub-network (refer fig. 6).	40
Figure 10(b): (continued) Contour Plots of the K_{mortar} solutions. Pressure solution taken from the interface between the 3(row) X 5(column) sub-network and the 3(row) X 6(column) sub-network (refer fig. 6).	41

CHAPTER 1: SUMMARY

This thesis has been divided into four chapters excluding the current chapter. Chapter 2 details the background information and introduces associated concepts and related information with this work. It also contains the reasons for undertaking this work/thesis and brief explanations of the way the work is to be carried out.

Chapter 3 explains the different techniques used in network generation with emphasis placed specifically on the statistical method used in this work. It also describes the solution technique that was employed in solving the network equations. The fourth chapter talks of the different types of approaches that have been used in testing the hypothesis of work, i.e. the finite difference approach and the finite element approach. It also contains a section describing in detail how linear mortar coupling was employed.

Chapter 5 deals with the observed results and discusses some of the reasons behind these observations. It has figures and tables highlighting the results. The last Chapter (six) gives concluding opinions and views of this work.

CHAPTER 2: BACKGROUND

2.1 INTRODUCTION

Flow and transport in porous media involving subsurface applications, such as hydrocarbon recovery, nuclear waste storage, and carbon storage requires accurate simulation for better understanding of the processes. Porous medium is made up of a solid space (matrix) and a void space (pores/throats). Fluid transport occurs in these pores and interconnecting throats forming the void space. The transport behavior in the porous media occurs at several scales (nanometer to kilometer), and developing models that bridge all of these scales can be challenging.

The oil and gas industry predominantly is focused on understanding the complex flow behavior in hydrocarbon reservoirs. Predominant methods employed utilize reservoir simulators which model fluid flow in the larger continuum scale (1 to 10^6 m). Computational limitations usually restrict modeling to the continuum scale by substituting semi-empirical models such as Darcy's law. Macroscopic properties (such as permeability) are often obtained through experiments, which can be tedious and time consuming.

A more fundamental scale is the pore scale (10^{-6} to 10^{-3} m). Pore-scale models capture the inherent connectivity and heterogeneity present at the pore level and provide a pore-level description and understanding of the porous material. These models can accurately capture pore-level fluid behavior, and often produce macroscopic properties that match experimental results, providing an efficient surrogate for such experimental tests. Advancements continue to be made to better describe pore structure and include more fundamental physics.

In this work we want to demonstrate methods which utilize the simulation-accuracies of pore-scale models and extend them into practical dimensions of continuum scale. The methods employed here utilize domain-decomposition principles where a large domain is solved as a series of smaller sub-domains. It is a divide and conquer strategy that overcomes computational restrictions in upscaling large pore-scale models. The problem being solved in this work involves single-phase, Newtonian fluids. The techniques introduced here can easily be extended to multiphase and non-Newtonian fluids in future work.

Probabilistic population techniques have been used in generating/creating large network models (domain $\sim 10^6$ pores). High-performance computing is used to obtain accurate results in these models. The domain is then decomposed into a hundred sub-network models (sub-domain), which are easier to manage computationally. These sub-networks are then coupled to each other iteratively to determine accurate boundary conditions for the sub-network models. Finite element mortars and finite difference methods have been employed to perform network coupling. The hypothesis is that the upscaled permeability will be more accurate than coupling use a simple finite-difference approach.

Four distinct permeability values have been calculated for a particular large network model: K_{true} , $K_{\text{mortar-constants}}$, $K_{\text{mortar-linear}}$, and K_{FD} . K_{true} is the computationally expensive permeability obtained by solving the domain (large network model) as a whole. This serves as a basis of comparison for accuracies of the coupling techniques. K_{mortar} (constants and linear) are the coupled permeabilities obtained by coupling the sub domains (sub-network models) using mortars. K_{FD} is obtained by solving the 2D Laplace equation use individual sub-network permeabilities for each block. Close matches between the true permeability (K_{true}) and the mortar-coupled permeabilities (K_{mortar})

demonstrates success of upscaling by using domain-decomposition coupling techniques compared to traditional coupling approaches (K_{FD}).

2.2 PORE-NETWORK MODELS

Network models are one type of pore-level approach for simulating flow and transport in porous media. Networks are created from digital data representing or extracted from actual porous materials. The pore network is represented as a system of pores (volume) having interconnecting throats (flow resistance). Fatt (1956) developed the model as an extension to over-simplistic existing models (such as bundle-of-tubes models) that did not mimic the complex pore structure of actual porous media. Grouping the tubes into a network with distributions in their radii was a better approximation to the pore geometries, resulting in more accurate solution to flow in the porous medium. Initial work on networks (Payatakes 1982; Koplik et al 1984; JD Chen et al 1985) involved regular (usually two-dimensional) grids which made quantitative determination of macroscopic parameters difficult. Advancements in computing provided a means for utilizing more complex and realistic networks.

Pore networks have been gaining popularity as a tool in predicting petrophysical properties of porous media. Pore-scale models provided a pore level understanding of fluid flow and this ability initiated them to be adopted within the oil and gas industry. Flow in porous media is dependent on the prevalent viscous and capillary forces existing in the media. Numerous works on predicting relative permeability curves using pore-network models have been undertaken. Bryant and Blunt (1992) presented a predictive way to calculate relative permeabilities using porous media made from a dense random packing of spheres.

Lopez and Blunt (2002) used single phase pore-network models in predicting the behavior of non-Newtonian fluids in porous media. The network models contained

irregularly shaped pores connected by throats that represented a series of different porous media. The relationship primarily being predicted was that between the apparent viscosity and the flow rate of the flowing fluid. The pore network results were compared against a series of experiments conducted on sand-packs and close agreements were observed in the results.

Thompson and Balhoff (2004) used pore-scale models in understanding the behavior of non-Newtonian polymers in propped fractures. The behavior of residual polymers in the propped fractures affecting the fracture permeability and fracture productivity was studied. The fracture clean-up problem is influenced by pore scale events in the reservoir and warranted pore-scale models in their study. This was more accurate than the currently existing continuum-scale models on fracture cleanup.

Gladkikh and Bryant (2006) used pore-networks in predicting the hysteresis during the fluid displacement cycle. Meniscus motion at the grain scale was maintained to be mechanistic and in the process automatically accounting for hysteresis. The model predicted that the hysteresis had a significant effect on the relative permeability and the resistivity index, n , used in the Archie equation (Bryant, 2006).

Pore networks have also been used as an alternative to scarce and reliable experimental data. Spiteri and Blunt (2008) used pore networks as predictive experimental reference, comparing against numerical simulations. The subject being investigated was the impact of trapping and hysteresis in the context of CO₂ sequestration projects in saline aquifers. Pore-network simulations maintain experimental accuracy with decreased effort and time in results generation.

Since the inception of pore-network models, a vast number of studies on various fields have been performed such as network characterization (Fatt, 1956; Payatakes 1982; Koplik et al 1984), relative permeability calculation (Bryant and Blunt, 1992), non-

Newtonian single phase flow (Lopez and Blunt, 2002; Thompson and Balhoff, 2004), fluid hysteresis (Gladkikh and Bryant, 2006) and experimental surrogates (Spiteri and Blunt, 2008). The practical scale to which the results can be applied is small and the problem associated with upscaling is usually not addressed fully in these applications. Pore-scale networks are often not large enough and larger pore-scale models are warranted in order to make realistic conclusions of the results observed. The models often fall into a scale which is lower than their representative elementary volume (REV). In this work we will be addressing this issue of the scale or the size of the pore network models. Rather than focusing on the various physics of fluid flow, the work is restricted to single-phase, creeping Newtonian flow and focus on upscaling the pore networks to larger scales. The upscaling techniques introduced here can easily be extended to multiphase or non-Newtonian fluids in future work.

One limitation to usual network modeling approaches is that the boundary conditions employed are simple; constant pressures or fluxes are imposed on each network face. The solution of the governing pore-level equations in the network model is dependent upon the boundary conditions imposed, which in turn affect the measured macroscopic property. Real boundary conditions depend on surrounding media which in-turn would result in more complex fluxes and pressure fields at those shared interfaces. In this work we demonstrate the use of more realistic boundary conditions. These boundaries are pressure and flux fields at the interfaces that better represent boundary conditions in actual in-situ porous media.

2.3 REPRESENTATIVE ELEMENTARY VOLUME (REV)

REV of a porous medium represents the smallest size (volume/area) of the sample capable of representing an actual physical rock. In order to determine petrophysical properties of a porous medium, samples of the porous media need to be measured /

analyzed. If the sample is too small, the reading of the petrophysical property tends to oscillate (fig 1). As we increase the sample size, the oscillation amplitudes begin to decrease. Eventually the sample size will become large enough that we begin to get consistent readings. This sample size is referred to as the representative elementary volume. For practical and consistent readings we need the samples to be larger than the REV (Bear, 1988).

Computational and imaging constraints restrict the size of network models. The models are often not large enough to be a representative elementary volume (REV). Network upscaling techniques used in this work pose a unique way of overcoming such limitations.

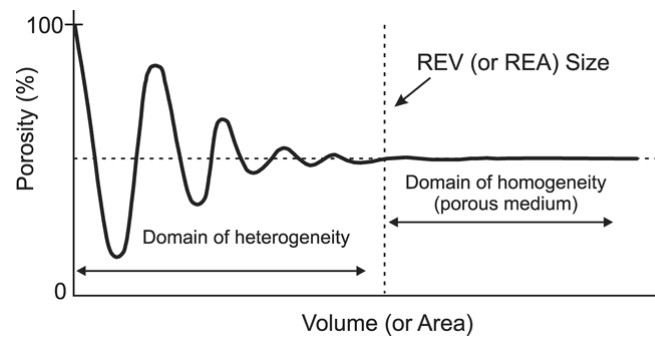


Figure 1: Visual depiction of the REV for a porous media with porosity as the measured quantity.

2.4 BOUNDARY CONDITIONS

The solution of the governing pore-level equations in the network model is dependent upon the boundary conditions imposed, which may in turn affect the upscaled macroscopic properties. Typically, the boundary conditions in pore-network modeling are simple; constant pressures or fluxes are imposed on each network face. However, the real boundary conditions depend on surrounding media which would result in more

complex fluxes and pressure fields at those shared interfaces. Accurate, efficient methods for coupling these models to surrounding media must be found, in the process replicating the boundaries that would be present in actual in-situ porous media.

2.5 FINITE ELEMENT METHOD

Finite element methods (FEM) or finite element analysis (FEA) is a numerical technique for approximating the solution of a partial differential equation (PDE) (Demkowicz, 1980). FEM is a good candidate in solving PDE's on complex domains having solution precision varying over the whole domain. For example, areas of interest such as near well bores or fractures in a reservoir can be more computationally expensive to model than the rest of the domain. Solving elasticity and structural problems in civil and aeronautical engineering in the 1950's proved to be increasingly complex and intricate. The need arose to develop innovative techniques to solve these complex problems. John Argyris (University of Stuttgart) and Ray W. Clough (Berkley) began developing and improving on the existing numerical technique of FEM, initially introduced by Alexander Hrennikoff (1941) and Richard Courant (1942). The technique gained widespread usage and fame when it was used by NASA for the development of their FEM software called NASTRAN.

FEM implements a divide and conquer technique, wherein the domain is discretized into smaller domains called meshes to achieve solution accuracy. These meshes can be created of triangular, rectangular or square elements. Such a feature enables FEM to handle complicated geometries/domains with relative ease. The discretized sub domains have basis functions defined; this reduces the larger problem into a series of smaller less complicated problems. The final solution results in a system of equations " $Ax=B$ ", where " x " is a vector and its size is equal to the degree of freedoms associated with the problem. Matrix " A " is visually shown in figure 2 and " B " is the load

vector. The solution (x) is a set of coefficients to the basis function defined across the sub domains.

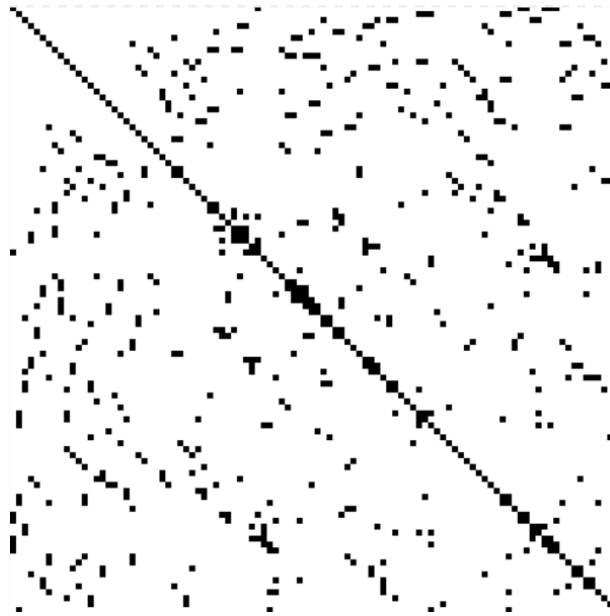


Figure 2: Diagonally dominant, sparse symmetric matrix (A) resulting while utilizing the FEM method. Each point on the figure represents a data value.

2.5.1 Mortar Coupling

Mortar coupling (Arbogast and Wheeler, 2006) is a domain decomposition approach that uses mortar finite elements to determine boundary conditions at shared interfaces in such a way that fluxes match weakly at that interface. The approach involves decomposing the domain into a series of smaller sub domains (Glowinski and Wheeler, 1988), which are coupled together using a low degree of freedom mortar space defined on a coarse grid. Utilizing higher order mortars and optimum mortar mesh sizes the accuracy of the solution can be enhanced. Some features of such a concept are local grid (h) and order (p) refinements (Wheeler, Arbogast, 2000; Bernardi, 1994). This is

especially useful as regions within the domain that require more attention can be modeled to have higher/optimum ordered basis functions or mesh sizes and the rest of the domain can have less intense mesh size and function order. Such a feature enables efficient usage of computational effort.

Mortars have been extended to coupling pore-network models (Balhoff et al, 2007) in a multiscale setting. In that work pore networks were coupled to an adjacent pore-network or continuum-scale model for single-phase flow. The work demonstrated that accurate pressure boundary conditions could be obtained, which resulted in accurate fluxes at the pore scale. In general, more accuracy was obtained using finer grids and higher-order mortars. However, the solution was less accurate if too fine a grid was implemented (too few pore throats were assigned to each mortar grid). A methodology was developed to perform upscaling, but macroscopic properties (e.g. permeability) were not calculated in that work. Here, the objective is to use mortar coupling to upscale permeability accurately without having to solve a single, large network.

2.6 FINITE DIFFERENCE METHOD

Similar to the finite element method, finite difference methods are also a numerical technique of approximating solutions to differential equations. This method employs the finite difference equations to approximate the derivatives of the differential equations. Three primary finite difference equations that are used are the forward difference, backward difference and the central difference equations. First order versions of these equations have been shown below. Higher orders of these equations follow similar precedence.

$$\begin{aligned}\Delta_h[f](x) &= f(x+h) - f(x). && \text{(Forward difference)} \\ \nabla_h[f](x) &= f(x) - f(x-h). && \text{(Backward difference)} \\ \delta_h[f](x) &= f(x + \frac{1}{2}h) - f(x - \frac{1}{2}h). && \text{(Central difference)}\end{aligned}$$

In this work we have used a reservoir simulator to couple the sub-networks together, using individual sub-network permeabilities. The hypothesis is that this traditional upscaling approach will result in inaccuracies because sub-network properties are not found through coupling. This simulator makes use of the finite difference equations to solve the 3D Laplace equation. The model has been created and solved using the UTCHEM reservoir simulator. UTCHEM, the University of Texas Chemical Compositional Simulator, is a three-dimensional, multiphase, multi-component, compositional, variable temperature, finite-difference numerical simulator. The simulator uses cell-centered pressures, harmonic mean for transmissibility, and a linear extrapolation boundary cells. The sub networks have been modeled as an aquifer having water as the only saturation. UTCHEM is used because it is capable of easily modeling no-flow and pressure-gradient boundary conditions.

2.7 OBJECTIVE

In this work we upscale permeability in large, heterogeneous media using physically-representative pore-scale network models. Probabilistic population techniques have been used in generating/creating the networks. High-performance computing is used to obtain accurate results in these models. The methods employed utilize domain-decomposition principles where the large domain is solved as a series of smaller sub domains. It is a divide and conquer strategy that overcomes computational restrictions in upscaling pore-scale models as a single domain. The large network is decomposed into hundred(s) of smaller networks (10x10 grid) and then coupled with the surrounding models to determine accurate boundary conditions. Mortars are used at shared interfaces to determine accurate boundary conditions. Finite element mortars are used to ensure flux continuities at interfaces by using a coarser grid mapped onto a much finer sub domain.

This upscaling technique has important implications for using pore-scale models directly in reservoir simulators in a multiscale setting. The problem being solved in this work is single-phase Newtonian fluid. The techniques introduced here can easily be extended to multiphase and non-Newtonian fluids in future work. The results compare favorably to the more computationally expensive (and impractical) approach of upscaling the media as a single model.

Four permeability values (K_{true} , K_{FD} , $K_{\text{mortar-constants}}$ and $K_{\text{mortar-linear}}$) have been calculated using the same large network model (domain). This probabilistically populated large network model has over a million pores.

- K_{true} is the computationally expensive permeability which is obtained by solving the large network model (domain) as a whole. This is denoted as the true/actual permeability and serves as a basis of comparison for accuracies of subsequent coupling techniques.
- K_{FD} is the permeability calculated by breaking up this large network model (domain) into smaller network models (sub-domains) and by coupling the sub-domains calculated permeabilities using the 2D Laplace equation.
- K_{mortar} (constants and linears) are the two permeabilities calculated by coupling the same sub-domains using constant and linear mortars respectively.

The upscaled permeability obtained by coupling using mortars (K_{mortar}) is found to be a closer approximation of the true permeability (K_{true}) rather than the traditionally approaches of computing the upscaled permeability (K_{FD}).

CHAPTER 3: NETWORK GENERATION AND SOLUTION

3.1 MODEL GENERATION

Pore-network models can be generated a number of ways and often describe the structure of real porous media. Quantitative values of petro physical properties can often be extracted from these pore networks can be obtained when the pore-structure is properly captured. Early methods of pore-network generation had largely been restricted to the direct measurements obtained by studying the thin rock sections (C. Lin et al, 1982, Doyen, 1988) and of serial stacks of thin rock sections (D.P. Lymberopoulos, 1992). Disadvantages of such a thin section approach involved man-hour intensive polishing/slicing/digitization, sample destructive nature of work. Direct measurement of the pore space has advanced considerably with the advent of X-ray computerized microtomography (CT) (B.A. Dowd et al., 1999), Scanning electron microscopy (ESEM), micro CT, Magnetic Resonance (NMR) and laser scanning confocal microscopy. These techniques can produce three-dimensional images of rock core samples, at uniform resolutions in all three directions, with the data sets being extremely rich in detail.

There are two generally used methods of pore-network extraction from real materials: the medial axis algorithm and the maximal ball algorithm. The medial axis (Lindquist et al., 1996) consists of discretizing the network by finding the medial axis in the pore-space domain. The maximum ball algorithm (Silin and Patzek, 2003) consists of creating spheres within the network and by assigning the larger spheres to be pores while the smaller spheres being assigned as throats.

3.1.1 Medial Axis Algorithm

The medial axis of an object is the path/skeleton along the geometrical centre of the object. The medial axis of a porous media provides simple and coherent information about the structure and geometry of the void space constituting the porous media. It serves as a tool in understanding the geometric structure of the porous media. The intensity variations in the digitized X-Ray tomography images are used to create the pores and throats of the network model. The first step in defining the medial axis is to apply a segmentation algorithm to separate the phases of the image based on the intensity values. A discrete “burn” algorithm is applied to the segmented binary image to obtain a discrete representation of the pore space (Sarkar and Siddiqui, 2009).

The medial-axis skeleton is subsequently obtained by inverting the image so that the background becomes the new foreground and vice versa and then computing the distance transform of the inverted image. The local maximum of the resulting image will represent points on the medial axis skeleton.

Lindquist et al (1996) developed algorithms to calculate effective pore body and throat radii and other geometric properties such as coordination number based on the medial axis of the pore space.

3.1.2 Maximum Ball Algorithm

The imaged data of 3D porous media is represented as voids and voxels, this representation is used as the input data in network extraction using the maximum ball algorithm. Maximal balls (MB) are defined as a set of voxels assembling a largest sphere. The conditions in which this sphere should be formed are 1) it must touch the grain surface 2) the sphere cannot be a subject of any other maximal ball. Every maximal ball possesses at least one voxel that is not contained in any other maximal ball; the aggregate

of all maximal balls defines the void space in a rock image. To define the topology, maximal balls are merged into clusters.

Two types of clusters are used single and multi clusters. In a single cluster, a principal maximal ball absorbs all its direct smaller neighbors. Whereas multi-clusters are extensions of single clusters, where the principal maximal ball absorbs the clusters of smaller neighbors in its domain. Pores are defined by the common principal maximal ball of each cluster and if a maximal ball is connected to two clusters, then it defines a throat. The radius, volume and the shape factor of the pores and throats are then calculated (Sarkar and Siddiqui, 2009).

3.1.3 Probabilistic Population

A goal of this work is to generate networks that are large in size ($\sim 10^6$ pores); the above two methods though popular for conventional sized networks pose to be computationally expensive in generating large networks. Here, probabilistic network generation techniques are used to create the large network. This technique involves the replication of observed probability distributions of certain key parameters. These probability distributions have been acquired through direct measurements from 3D images. The details of methods and techniques used to breakdown the 3D image into distributions have been discussed by Sok et al. (2002). The parameters for the distributions are of typical Berea sandstone (Venkatarangan, 2000). All simulations in this work follow distributions observed in Berea.

Key parameters in real media follow particular probability distributions recreation of these probability distributions will enable in the construction of the network model representing that particular rock. These parameters are coordination number (C), throat length (L) and throat radii (R). The coordination number refers to the number of other

pores to which that particular pore is connected. Typical Berea sandstone has the below shown distributions (Venkatarangan, 2000) for length, radii and coordination number and these particular distributions have been used in this work. Figure 3 visually shows these distributions.

- Coordination Number $P(C) = 10^{-L/a}$ (Exponential) (1)
- Throat Length $P(L) = 10^{-L/b}$ (Exponential)
- Throat Radii $P(R) = R \times e^{-R^2/c^2}$ (Rayleigh)

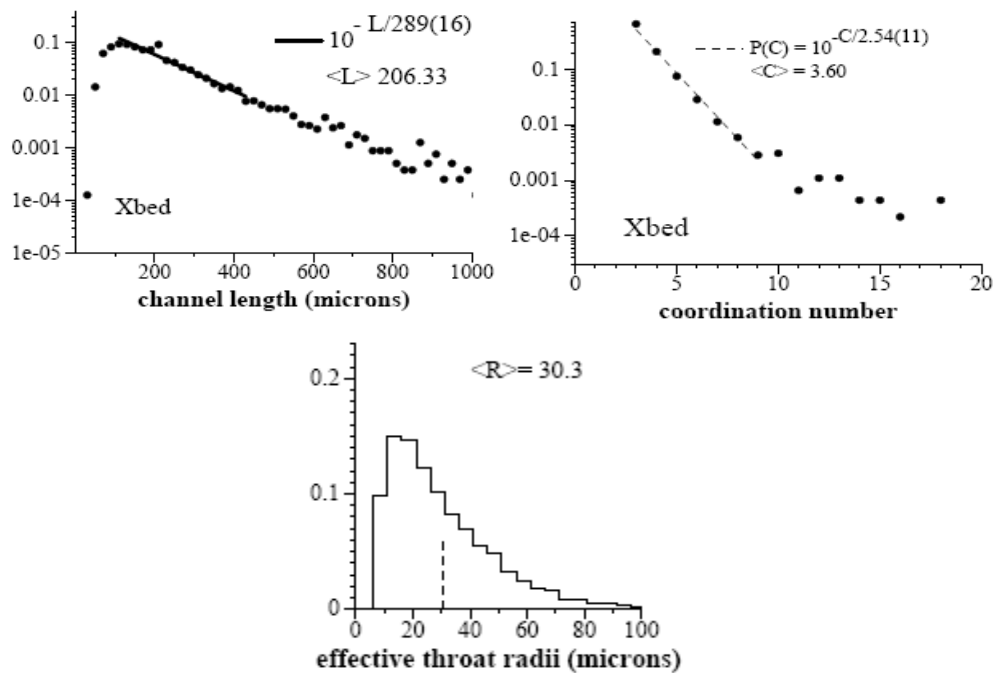


Figure 3: Probability distributions (Berea) used in model generation (Venkatarangan 2000)

The values a , b and c are variables defining the coordination number throat length and radii distributions respectively. In this work the variables a , b and c are arbitrarily

chosen (to create anisotropy) around the average value for Berea sandstone. Using this probabilistic population technique two different networks have been created, network A and network B. The parameters a , b and c used in generating them are shown in table A.1. These two different networks represent two different network cases.

A Monte Carlo sampling technique is used to re-create the probability distributions using uniform random number generators available in commercial software's. Let $p(rnd_1)$ and $p(x_1)$ be the probability distributions of the uniform and subject distribution and $F(rnd)$ and $F(x)$ the integrals of these probability distributions. The fundamental basis of the Monte Carlo technique is to equate $F(rnd_1)$ (Refer Figure 4) to be equal to $F(x_1)$, then through this relation a point of connection is made between $p(rnd_1)$ and $p(x_1)$. Random selection of “ rnd_1 ” in a uniform distribution is mapped onto a “ x_1 ”, that represents the original $p(x)$ probability distribution. A random number, rnd_1 , is chosen by the compilers uniform distribution subroutine.

This process is equivalent to equating the hatched areas under the $p(rnd)$ and $p(x)$ curves in the fig. 4. The total areas under the $p(rnd)$ curve from 0 to 1 and under the $p(x)$ curve from a to b are both equal to 1. In this way, a choice of rnd chooses a unique value x_1 of the distribution of interest. As a large number of random numbers, rnd_1 , are chosen, the set of associated x_1 values will be sampled from $p(x)$ probability distribution in a non-biased way such that the histogram of chosen x_1 values will recreate the original function $p(x)$.

Mathematically, the equivalence of $F(rnd_1)$ equal $F(x_1)$ can be stated as:

$$\int_a^{x_1} p(x) dx = F(x_1) = F(rnd_1) = \int_0^{rnd_1} p(rnd) d(rnd) = rnd_1 \quad (2)$$

Or more simply

$$\int_a^{x_1} p(x) dx = rnd1 \quad (3)$$

After evaluation of the integral above, the expression can be rearranged to solve for x_1 in terms of $rnd1$. Using this equation/relation, for every choice of “ $rnd1$ ” from the uniform distribution shall yield an equivalent value “ x_1 ” representing the probability distribution $p(x)$ (Steven Jacques, 1998).

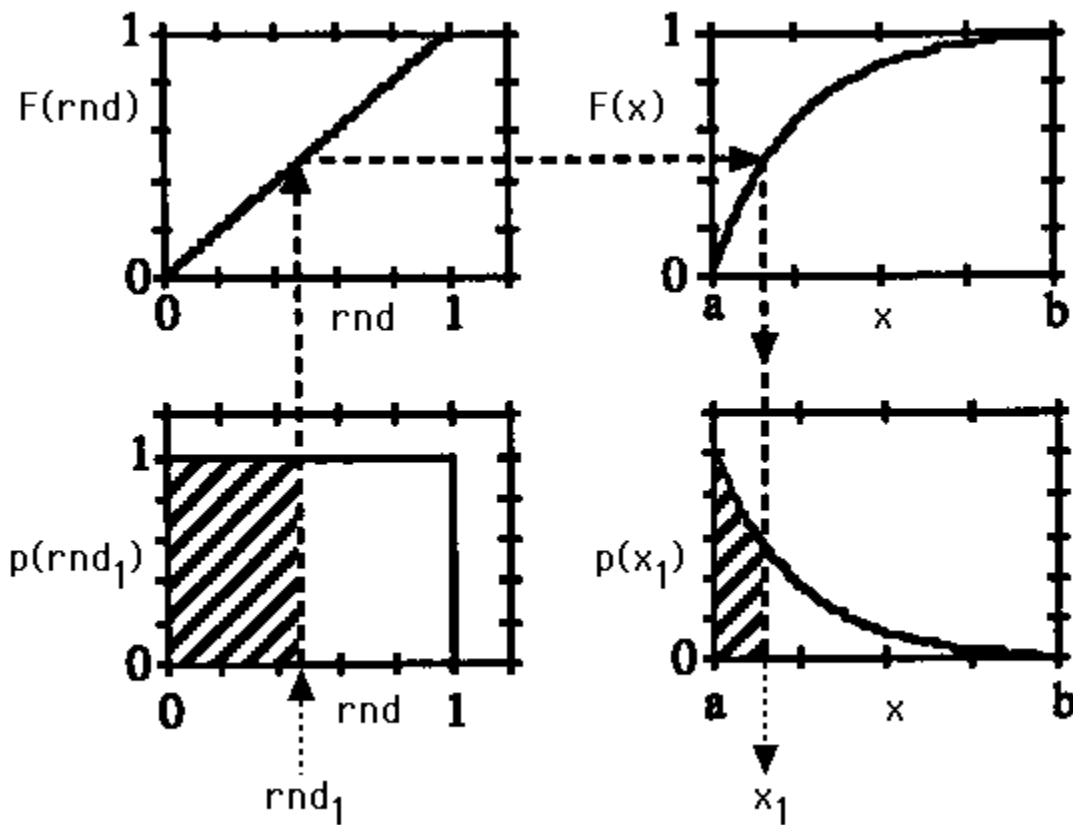


Figure 4: The above figure illustrates the connection between $p(rnd_1)$ and $p(x_1)$ via the equation of $F(rnd)$ equal $F(x)$. $p(rnd_1)$ and $p(x_1)$ are the probability distributions of the uniform and subject distribution and $F(rnd)$ and $F(x)$ are the integrals of these probability distributions. (Steven Jacques, 1998)

3.1.4 Detailed Description of Network Generation

Network models are generated here by recreating the probability distributions of key parameters such as coordination number, throat length and throat radii. Only three probability distributions are used; they are the coordination number for each pore, throat radii and the throat lengths. Equation 1 describes these three probability distributions. Monte Carlo sampling techniques as described in the previous section have been used in generating the probability distributions, using uniform probability distributions present in programmable software's.

The number of pores and the coefficient's for the probability distributions (a , b , and c ; eqn. 1) need to be specified explicitly; as they are intended to be varied for the different networks that can be created. A particular network has to be specified with the particular number of pores and values of a , b and c for a particular pore structure. Varying these quantities creates different networks. In order to create two different networks two different sets of parameters a , b , c and number of pores should be specified.

Pores are placed randomly within the network space. Boundary pores have been created by moving pores close to the boundary physically onto the boundary. Using the distributions for the coordination number the number of throats in the network can be determined. Using the data of pore locations, coordination number, throat length and number of throats the neighboring pore to which the pore has to be connected is determined. To decrease computational effort of searching the neighboring pore, emphasis is given on searching for the neighboring pore in the immediate vicinity rather than other portions of the network.

Final aspects of network generation are in using data of the throat lengths and radii to calculate the conductivity in each of the throat using the Hagen-Poiseulle equation (eq. 4).

The basic algorithm is as follows:

- Determine the parameters a , b , c (eqn. 1) and the number of pores, by interpreting the digital data from imaged porous media.
- Use the coordination number probability distribution in assigning the coordination number for each pore, and subsequently in determining the number of throats.
- Assign random locations to the pores within the network and classify them into interior and boundary pores.
- Use the information on pore locations, coordination number, throat length and number of throats to determine which neighboring pore a pore has to be connected to.
- Assign conductivities of all the interconnecting throats based on their radius and length.

3.2 MODEL SOLUTION

The Hagen-Poiseulle equation is used to describe single-phase, creeping flow in throats in the pore-network model. In this work the fluid flow is single-phase Newtonian and accordingly the assumptions applied to the Navier-Stokes are 1) Flow is laminar, viscous and incompressible in the throats 2) Flow is through circular cross-section throats whose length is significantly longer than the diameter 3) Flow is steady state. The derived Hagen Poiseulle (eq. 4) equation is a relationship between pressure drop and flow in long cylindrical throats.

$$Q = \frac{\pi r^4 (\Delta P)}{8 \mu L} \quad (4)$$

Applying the Hagen-Poiseuille equation to all throats in the network results in a system of N equations having N unknowns (N being the number of pores). The solution of this system under applied boundary conditions results in the unknown pressure values for each pore. The overall flow Q_{total} across the network is calculated by applying the Hagen-Poiseuille equation across each boundary throat. The permeability of the entire network (K) is in-turn calculated by solving for “ K ” using Darcy’s law (eq. 5). Where L_{model} , ΔP and A are the length, pressure drop and area of the entire network model.

$$K = \frac{Q_{\text{total}} \mu L_{\text{model}}}{A (\Delta P)} \quad (5)$$

3.3 DOMAIN DECOMPOSITION (DIVIDING THE PORE NETWORK)

Large networks ($\sim 10^6$ pores) which are probabilistically populated and spatially correlated have been created. These networks are highly heterogeneous / anisotropic possessing large variations in the distributions of the throats sizes and pore numbers. These variations are abrupt and create abrupt changes in the local-permeability of the porous medium. The purpose is to mimic naturally occurring rock which is highly anisotropic and heterogeneous. A visual depiction of sub-networks being created along regions of abrupt changes and arranged to form the larger parent network is shown in figure 5.

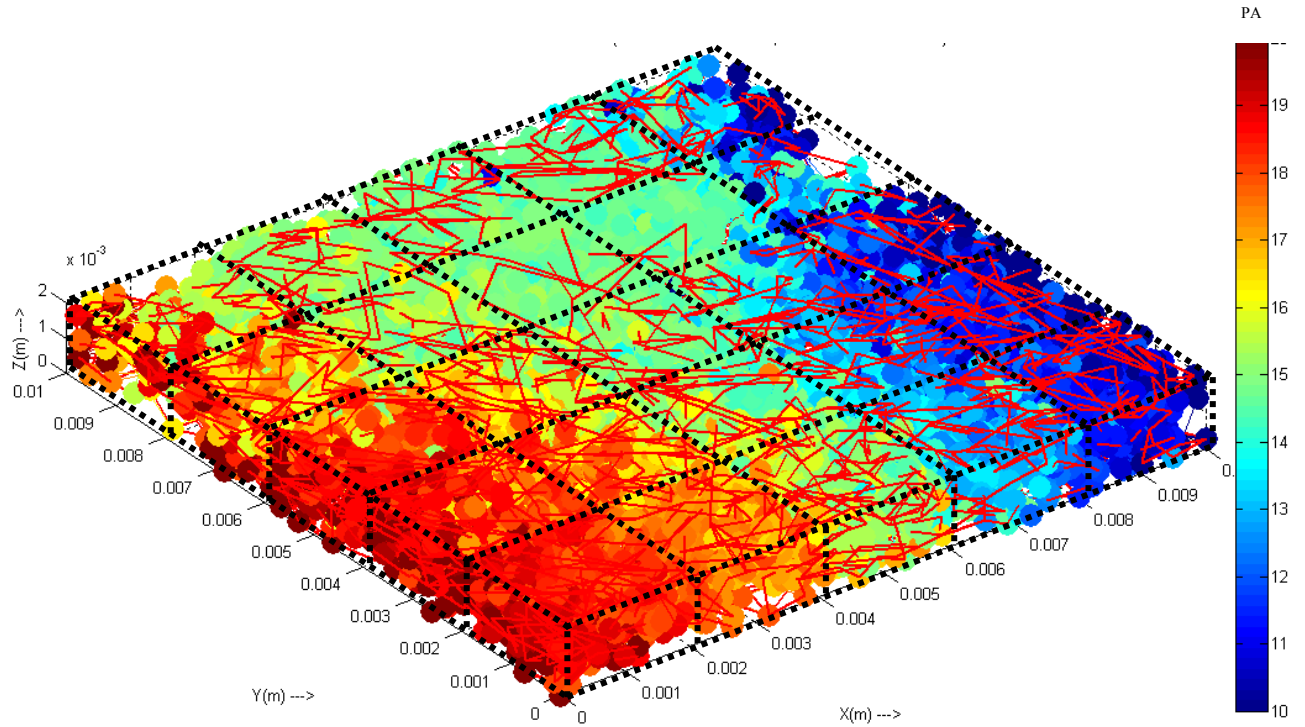
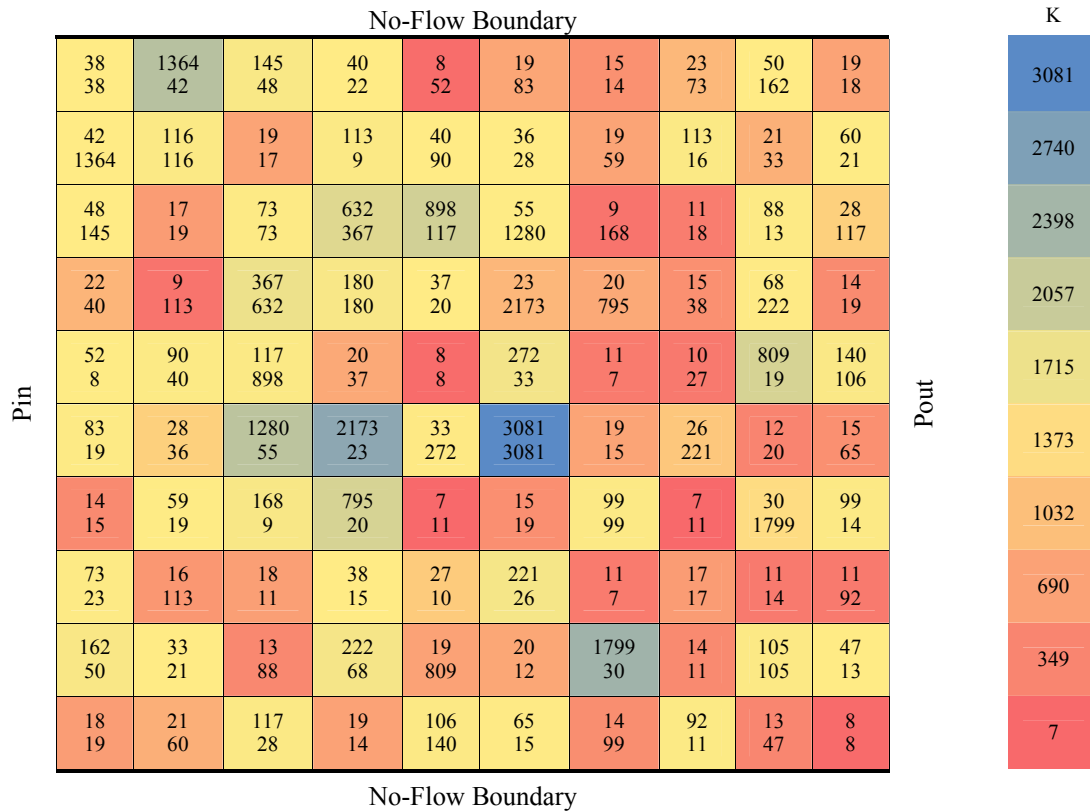


Figure 5: Example large network divided into 5x5 sub-network grids (total pores = 4720, range = 70-400 pores)

Here the large network is divided into several smaller sub-networks that are easier to manage computationally; they are divided naturally at these places of abrupt changes in permeability. In this work we divide the large network into 100 sub-networks comprising a 10x10 grid. The network is divided by generating small sub-networks, which are aligned or spatially located with respect to each other in such a way so that their distributions match up with the distributions of the parent large network model. Figure 6 visually shows the permeability variations (heterogeneity) in the 10x10 small sub-networks in networks A and B. Network A and B represent two independent numerical experiments (table A.1 and equation 1 contain probability values).

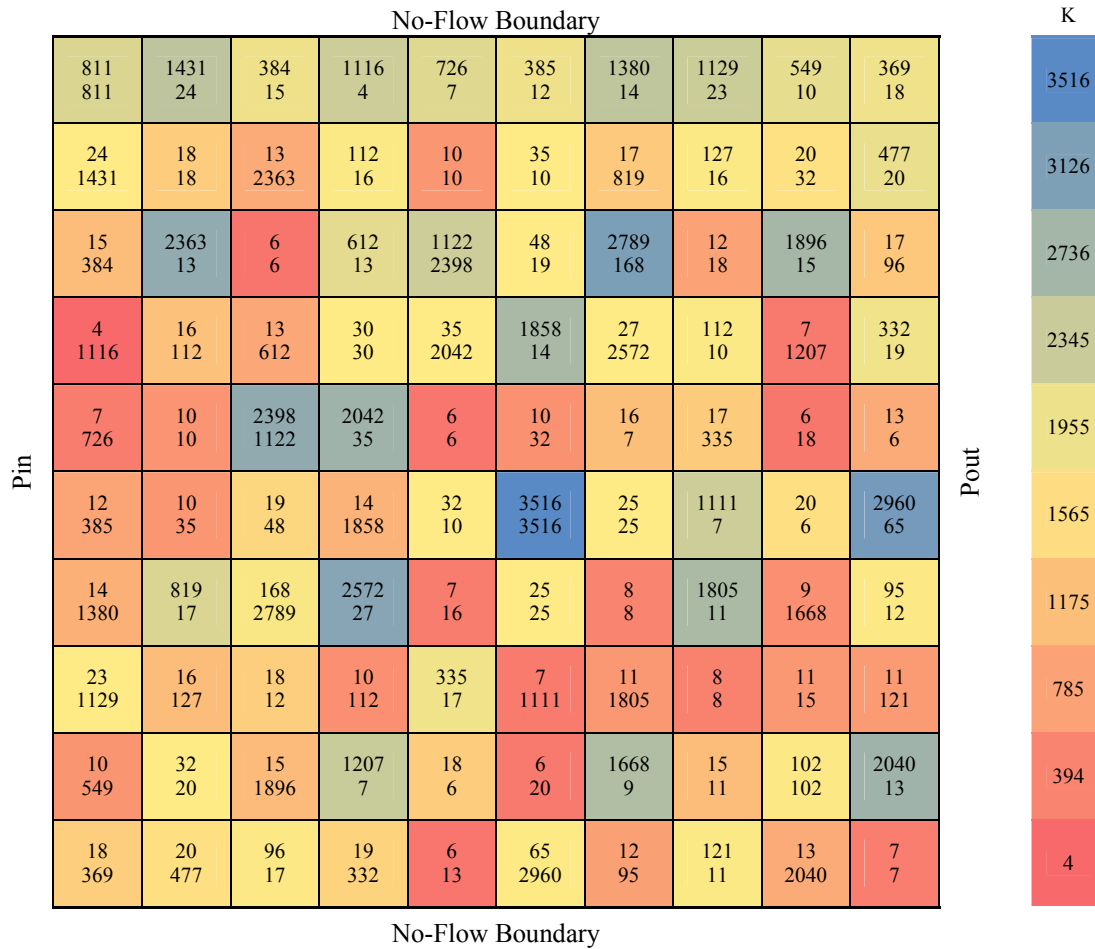
3.4 FINITE DIFFERENCE

Finite difference reservoir simulators are commonly used for simulating flow and understanding reservoir characteristics of oil and gas reservoirs. Other types of simulators are streamline and finite element simulators. A simple black oil finite difference simulator employs the finite difference approximations in solving the unsteady state three-phase diffusivity equation. The reservoir domain is divided into grids with appropriate boundary conditions allocated for solution convergence. The goal here is to upscale permeability of the large domain by piecing together the sub-network permeability. Ideally, the upscaled permeability would closely match the permeability obtained by solving the entire network.



(a)

Figure 6: Plot showing the permeabilities of the 10x10 sub-networks, (a) Network A (b) Network B. In each block, the values on the top are the permeabilities for the K_{xx} configuration and values at the bottom are the permeabilities for the K_{yy} configuration.



(b)

Figure 6: (continued) Plot showing the permeabilities of the 10x10 sub-networks, (a) Network A (b) Network B. In each block, the values on the top are the permeabilities for the K_{xx} configuration and values at the bottom are the permeabilities for the K_{yy} configuration.

In this work the single-phase steady-state diffusivity equation (eq. 6) in Cartesian coordinates is solved. The problem domain consists of the 10x10 sub-networks created out of the large network model (having $\sim 10^6$ pores). Each of the small sub-networks has a unique permeability ranging from 7md to 3000md, representing a very heterogeneous (and anisotropic) problem domain (fig. 6). Solving the diffusivity equation applied on the sub-networks results in individual pressure values. Using this pressure solution the overall flow and subsequently the overall permeability K_{FD} is calculated using Darcy's law.

$$\nabla \cdot \left(\frac{k\rho}{\mu} \cdot \nabla \phi \right) = 0 \quad (6)$$

The model has been created and solved using the UTCHEM reservoir simulator. UTCHEM, the University of Texas Chemical Compositional Simulator, is a three-dimensional, multiphase, multi-component, compositional, variable temperature, finite-difference numerical simulator. The simulator uses cell-centered pressures, harmonic mean for transmissibility, and a linear extrapolation boundary cells. The domain was modeled as an aquifer having water as the only saturation. UTCHEM is used because it is capable of easily modeling no-flow and pressure gradient boundary conditions.

3.5 FINITE ELEMENT MORTARS

A limitation of the finite-difference approach above is that sub-network permeability values were obtained using simple boundary conditions – that do not reflect the surrounding media. Here, the sub-networks are coupled using mortars, so that more accurate boundary conditions are used. Coupling of sub domains is only possible provided the sub-domain space has a finer mesh (h) than the coarser mortar space. The mortar solution is found by determining the coefficients for the basis functions describing

the mortar space. The basis functions (p) vary in order hierarchically from constant, linear, quadratic and cubic (to even higher) order functions. Here constant and linear basis functions have been used and the mesh sizes have been varied from a 1x1 grid to a 4x4 grid. Solution convergence is ensured by the optimum choice of either function order (p) or mesh size (h).

3.5.1 Coupling with Mortars

The approach for coupling pore-scale network models using mortars is outlined in Balhoff et al. (2009), but a summary of the iterative approach is included here for clarity.

- Assign basis functions, $\varphi(x,y)$, for the mortars. Constant mortars have basis functions equal to one; higher order mortars are more complicated functions of x .
- Provide an initial guess the coefficients (α_1, α_2 , etc.) of the basis functions for both constant and linear mortars.
- Calculate the interface pressure field $P(x,y)$, based on the coefficients and basis functions using the below relation.

$$P_{m,i} = \alpha_{m,1} * \varphi_{m,1} + \alpha_{m,2} * \varphi_{m,2} + \alpha_{m,3} * \varphi_{m,3} + \alpha_{m,4} * \varphi_{m,4} \quad (7)$$

- Using the equation for the pressure field (eq. 7), determine the individual interface boundary pressures using the x and y coordinates of the boundary pore.
- Match the weak mortar flux across the interface using the below relation

$$\int_{\Delta} q_L * \varphi + \int_{\Delta} q_R * \varphi = 0 \quad (8)$$

- The flow across the interfaces are point sources and can be treated as point impulse functions, the above relation can be reduced to the below analogy. The flow q_L and q_R are calculated using the Hagen-Poiseule equation

$$\sum q_L * \varphi + \sum q_R * \varphi = 0 \quad (9)$$

- The above relation leads to a non-linear system of M equations having M unknowns.

This is represented below

$$\begin{aligned}
 q_L^* \varphi_1 &= q_R^* \varphi_1 \\
 q_L^* \varphi_2 &= q_R^* \varphi_2 \\
 q_L^* \varphi_3 &= q_R^* \varphi_3 \\
 q_L^* \varphi_4 &= q_R^* \varphi_4 \\
 &\vdots \\
 &\vdots \\
 &\vdots \\
 q_L^* \varphi_M &= q_R^* \varphi_M
 \end{aligned} \tag{10}$$

- Solve for the unknowns ($\alpha_1, \alpha_2, \text{etc.}$) using the Newton Rhapsods method by calculating the partial derivatives ($\partial F_m / \partial P$) and constructing the Jacobian.
- Solve the resulting system of equations; calculate the $\partial \alpha_m$ and the resulting coefficients for the basis function or the pressures directly in the case of constants.
- Check for solution convergence and calculate the $K_{\text{mortar-constant}}$ and $K_{\text{mortar-linear}}$
- Solution converges in one iteration for both constants and linears since flow is single-phase, creeping, and Newtonian. More complex flows (e.g. multiphase) would be nonlinear and therefore require more iterations for convergence.

3.5.2 Coupling Example Using Linear Mortars

Linear mortars use linear basis functions in constructing/approximating the solution. In this section the details of how mortar coupling is performed using a 1x1 linear mortar mesh on two simple sub networks as an example.

Figure 7(a) shows the two sub-networks with the 1x1 linear mortar mesh and Figure 7(b) shows the 1x1 mortar mesh in detail showing the geometry of the basis functions. Let us consider two boundary pores $BP1$ and $BP2$ at locations $x1, y1$ and $x2, y2$

on their respective interfaces of sub-network 1 and 2 respectively. The equations for the four linear basis functions in dimensionless units are as follows:

$$\varphi_1(x, y) = (1 - x) * (1 - y) \quad (11)$$

$$\varphi_2(x, y) = x * (1 - y)$$

$$\varphi_3(x, y) = (1 - x) * y$$

$$\varphi_4(x, y) = x * y$$

Where, $0 < x < 1.0$ and $0 < y < 1.0$

The pressure solution for boundary pores *BP1* and *BP2* is dependent on their x, y location on the interface. Mathematically it is calculated using the below equations.

$$P_{BP1}(x1, y1) = \alpha1 * \varphi_1(x1, y1) + \alpha2 * \varphi_2(x1, y1) + \alpha3 * \varphi_3(x1, y1) + \alpha4 * \varphi_4(x1, y1)$$

$$P_{BP2}(x2, y2) = \alpha1 * \varphi_1(x2, y2) + \alpha2 * \varphi_2(x2, y2) + \alpha3 * \varphi_3(x2, y2) + \alpha4 * \varphi_4(x2, y2)$$

(12)

The coefficients of the basis functions ($\alpha1, \alpha2, \alpha3, \alpha4$) are guessed in order to approximate a solution for the boundary pressures. The approximated pressure solution is used in calculating the flow across the sub-network using the Hagen-Poiseuille equation for each boundary pore. The criterion for solution convergence in mortar coupling is that fluxes at the interface should match weakly. Let q_L be the flow through sub-network 1 and q_R through sub-network 2 respectively. The weak form of the mortar solution at the interface is written as

$$\int_{\Delta} q_L * \varphi + \int_{\Delta} q_R * \varphi = 0 \quad (13)$$

Expressing this relation numerically, equation 12 can be written as

$$\Sigma q_L * \varphi + \Sigma q_R * \varphi = 0 \quad (14)$$

Equation 14 denotes the mortar solution as the summation of the flows in each of the boundary pores at the network interface multiplied with their basis functions. Writing equation 14 for our case where there is only one boundary pore per interface, we get the below set of equations.

$$\begin{aligned} q_L(x1, y1) * \varphi_1(x1, y1) + q_R(x2, y2) * \varphi_1(x2, y2) &= 0 \\ q_L(x1, y1) * \varphi_2(x1, y1) + q_R(x2, y2) * \varphi_2(x2, y2) &= 0 \\ q_L(x1, y1) * \varphi_3(x1, y1) + q_R(x2, y2) * \varphi_3(x2, y2) &= 0 \\ q_L(x1, y1) * \varphi_4(x1, y1) + q_R(x2, y2) * \varphi_4(x2, y2) &= 0 \end{aligned} \quad (15)$$

This results in an M set of equations with M unknowns, in this case four equations and four unknown alphas. The system is nonlinear as the flow (q_L and q_R) is a function of alpha (the unknown solution). Nonlinear equation solving techniques have to be used in determining the solution. In this work the non-linear set of equations has been solved using the Newton-Raphson method.

Forward difference approximation is used in calculating the partial derivatives numerically. These derivatives are used to create the Jacobian. The load vector is calculated using the relationship in equation 15. The solution of the Jacobian and the load vector results in the correct solution of alphas ($\alpha1, \alpha2, \alpha3, \alpha4$). Newton-Raphson's method is an iterative method of problem solution, as a single phase fluid is being solved in this work; the solution converges in one iteration.

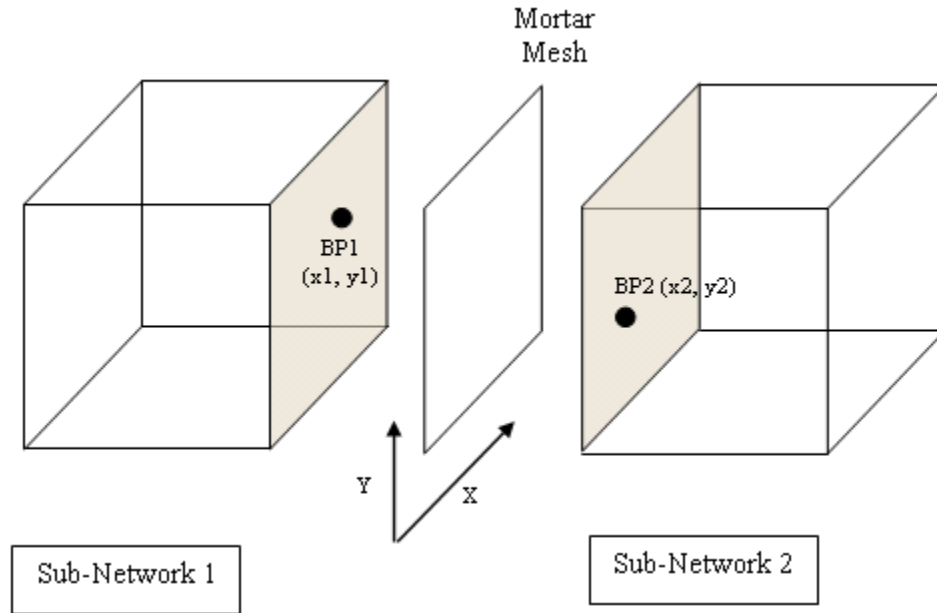
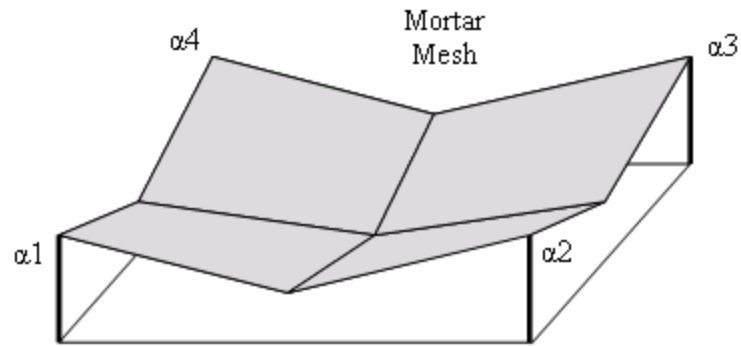


Figure 7(a): Illustration of two sub-networks (sub-network 1&2) showing their interface boundary with example boundary pores BP1 and BP2 on sub-network 1&2 respectively. The interconnecting mortar mesh (1x1 linear mortar) is also shown in between the sub-networks. Note the X and Y axis.



(b)

Figure 7(b): Illustration of the 1x1 mortar mesh, note the alphas ($\alpha_1, \alpha_2, \alpha_3, \alpha_4$) at the four corners and also geometrical depiction of the basis functions in grey shading.

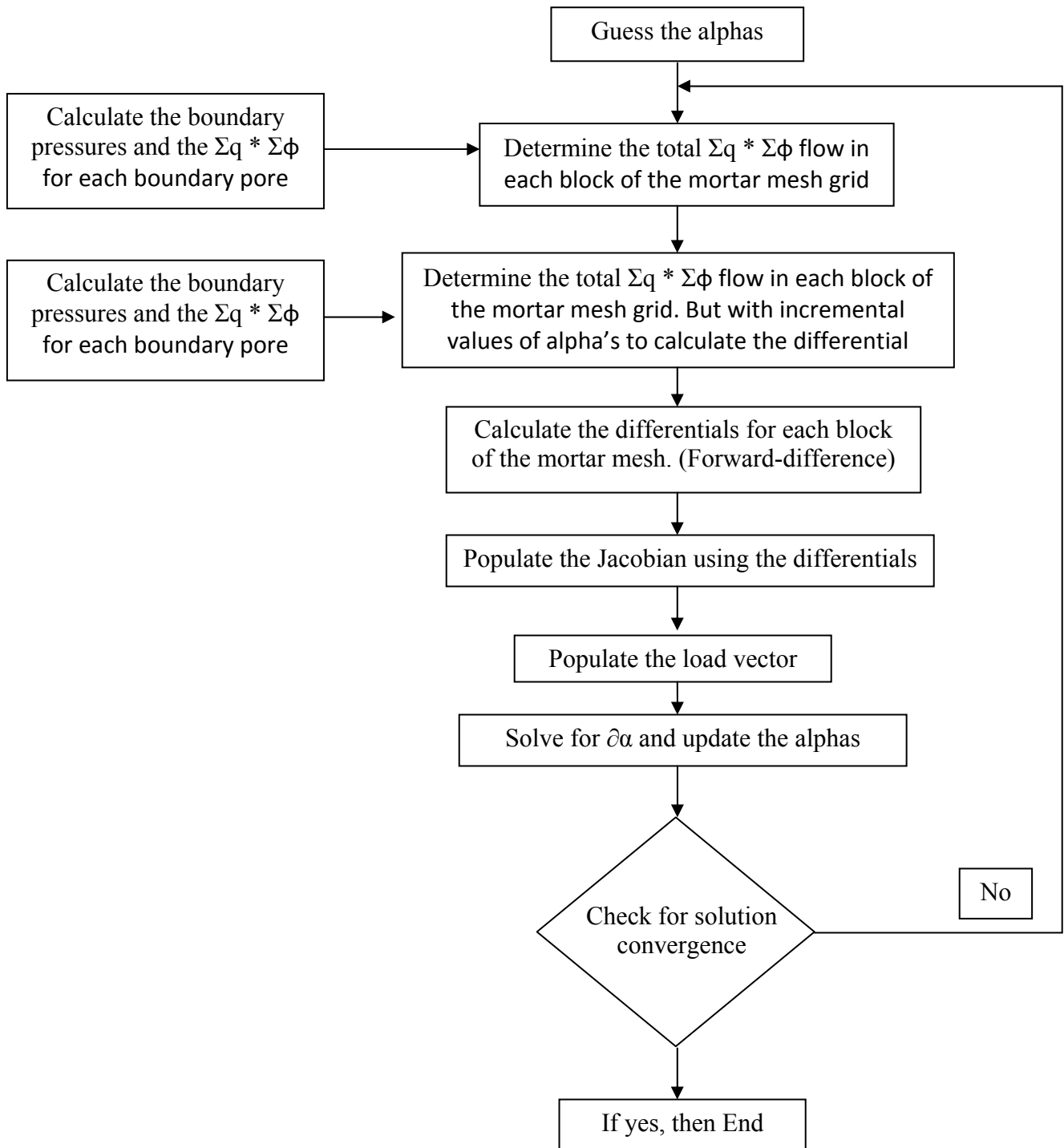


Figure 8: Flow chart showing mortar coupling logic.

CHAPTER 4: RESULTS/DISCUSSION

4.1 MILLION PORE LARGE NETWORK

Two large networks (network A and B) have been created, using the statistical techniques described in the previous sections. Network A has 1,000,088 pores and network B has 1,000,071 pores. The two networks are both heterogeneous/anisotropic in their construction and represent two different, heterogeneous Berea rock samples. The statistical properties of the two networks are similar, but network B is much more anisotropic.

The dimensions of each network is 0.02m x 0.02m x 0.002m in the x, y and z directions respectively. The network was constructed in such a way that abrupt changes in pore structure occurred at regular intervals. Each of the 10 x 10 x 1 sections (0.002m x 0.002m x 0.002m) have unique pore and throat size distribution as well as average coordination number (eq. 1). Table A.1 summarizes the range of values used in the models. The abrupt and varying permeability creates an overall heterogeneous network. Figure 6 illustrates the permeability variations for the sub-networks for network B, which can vary by two orders of magnitude.

In these large network models, flow is solved in the usual way. A pressure gradient is imposed in one direction and no flow boundaries imposed on the four faces (one could argue that these boundary conditions are still arbitrary - and they are – but they are more realistic at this larger scale). The pore-level equations are subsequently solved, which gives pore pressures and fluxes. The total flow in the model can be calculated and the permeability determined via Darcy's law. We refer to this as K_{true} and is the standard of comparison for the upscaling results described below. The K_{true} values

have been determined in both the x and y directions for both networks (A and B). Their results have been tabulated table-2.

Table 1 Permeability comparisons between K_{true} , K_{mortar} and K_{FD} . Number of pores in network A is 1,000,088 pores and network B has 1,000,071. Probability distribution parameters are given in Table A.1.

		K_{true}	K_{FD}	$K_{\text{mortar-constant}}$				$K_{\text{mortar-linear}}$			
				1x1	2x2	3x3	4x4	1x1	2x2	3x3	4x4
		md	md	md	md	md	md	md	md	md	md
Network A	Kx	37.54	32.39	65.52	49.27	43.44	40.35	40.01	39.05	38.09	36.9
	Ky	44.69	36.21	80.23	59.94	53.34	49.2	48.62	47.29	46	44.55
Network B	Kx	101.04	81.08	159.58	128.46	110.73	105.89	106.52	104.08	101.04	97.4
	Ky	37.1	28.99	54.24	42.83	37.93	37.04	37.06	36.48	35.7	34.79

4.2 FINITE DIFFERENCE SIMULATION

Our objective is to upscale permeability by decomposing the domain and solving several smaller problems. The network is divided into smaller sections using the positions of abrupt pore-structure changes as natural dividing points. Both networks (A and B) have been divided into 100 smaller sections on a 10 x 10 x 1 grid. Each of the sub-networks contains its own unique parameters as shown in Table A.1.

A traditional hierarchal upscaling approach would involve the calculation of permeability of each sub-network, followed by upscaling of the fine grid to a coarse grid. Here, we calculate the permeability of each sub-network in the usual way. The permeability of the sub-networks varies from 7 md to 3000 md for network A, and between 4 md to 3516 md for network B. Network B is more anisotropic than Network

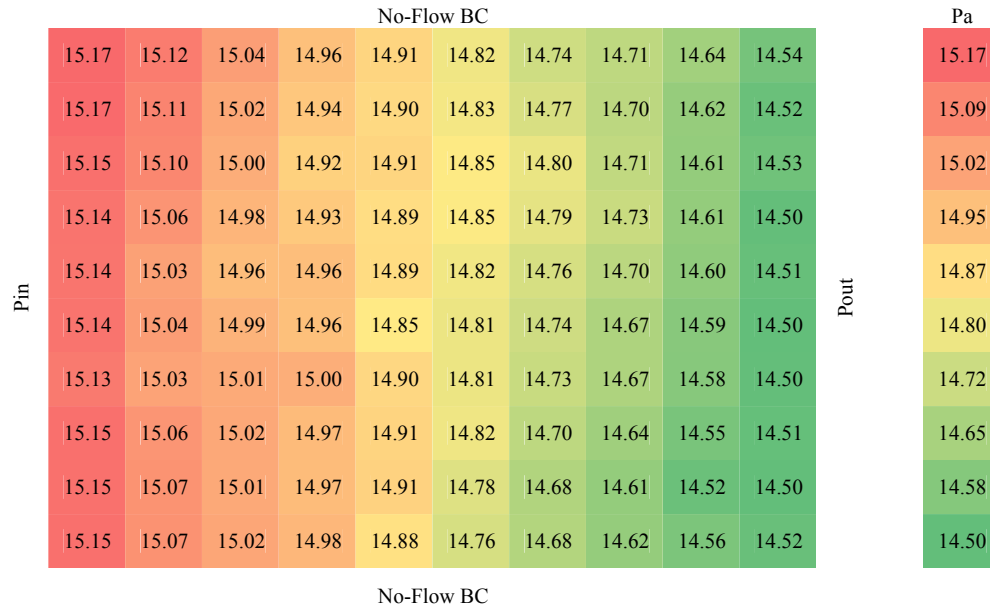
A; this is achieved by the distributions of high and low permeability networks into channels having high and low flow regimes.

The sub-network permeabilities are placed on the fine grid and then upscaled to a single, coarse permeability. The finite difference simulation to determine K_{FD} is performed using the academic simulator UTCHEM.

Using the Darcy equation the net flow across the model is calculated as well as the upscaled permeability, K_{FD} , which are shown in table 1. It is observed that in network A the K_{xx} and K_{yy} permeability is 14% and 19% less respectively than the true permeability (K_{true}) and in case B, 20% and 22% less than the true permeability, respectively. A likely reason for lower permeability values is because the transmissibility's of the diffusivity equation are being calculated by using the Harmonic mean in UTCHEM. Figure 9(a) and (b) visually shows the pressure variations obtained by the finite difference solution for network A and B.



(a)



(b)

Figure 9: Contour plots of (a) network A and (b) network B showing the pressure variations for the finite difference solution. The parameters in colored boxes are pressures.

4.3 MORTAR-COUPLED RESULTS

The upscaled values of permeability calculated using the finite difference approach may not be sufficiently accurate. An alternative approach is proposed here in which the sub-networks are coupled at shared boundaries using finite element mortars (constant and linear) as described in previous chapter. The goal is to obtain better estimates of permeability by implementing more accurate boundary conditions on shared interfaces.

Flow was modeled through each sub-network (with boundary conditions obtained through mortar coupling). Permeability is then extracted using the total flow through large domain and Darcy's law. The calculated permeability for each network is shown in Table 1. As expected the mortar solution generally increases in accuracy with increasing elements of the interface mesh (h -refinements) and with increase in the order (p -refinements). It is observed that mortar coupling achieves accuracy in its coarse grid to that of the sub-domain fine grid by using higher order basis-functions. The K_{xx} and K_{yy} calculated using a 4x4 grid of linears results in a -1.7 % error for network A and -3.6% error for network B. Similar results were observed in the other simulations. Table 1 contains a more detailed tabulation of the individual errors observed. The network A linear solution is closer to the true solution than the constant solution as expected. Using higher order basis functions (linear) provides more accurate approximation of the problem and lesser errors which is seen in the results of network A.

In network B higher errors are observed with finer mesh sizes. This is due to over meshing resulting in the finite element mesh being too fine. A too fine a mesh is faced with issues such as too few pores in some of the elements of the mesh, and coupling at that scales results in error. A catastrophic case results in mesh refinement so small that

some interface grids contain no pores. Physically, no flow would be entering on one side and it is impossible to match fluxes. Numerically, the Jacobian would become singular.

The resulting boundary conditions at the sub-network interfaces are heterogeneous, reflecting the effect of surrounding media. 2D surface plots of the pressure field at one interface (network A) is shown in Figure 10(a) (true solution) and Figure 10(b) (mortar-coupled solutions). This pressure field is taken from the interface between the 3(row) \times 5(column) sub-network and the 3(row) \times 6(column) sub-network (refer fig. 6). These plots visually show the convergence of the pressure solution. Finer or optimum meshing sizes qualitatively increase the solution accuracy, with the 4x4 (network A) mesh having the best match to the true solution (Figure 10(a)). Finer/optimum grids or higher orders or closer approximations of the interface pressure field produces solutions (permeability) which are closer to actual solutions (K_{true}). These contour maps have been plotted from a network A interface, where there is no increase in error with decrease in mesh size.

Approximating flux continuity by defining single pressure (K_{FD}) values using simpler boundary conditions around the network results in a less accurate approximation of the interface pressure field and subsequently varying heterogeneous flux. The in-situ rock and also its surrounding rock are not homogeneous but rather have varying heterogeneous petrophysical properties. Fluid flow through the throats constituting the rock will not be uniform over the interfaces but rather dependant on pore-level variations in petrophysical properties (throat dimensions and conductivity. Certain pores on the interface have larger throats/higher-conductivities as a result higher-flow than other pores on the interface which can have smaller throats/lower-conductivity with lower-flow. Quantitatively demonstrating the need for pressure fields as boundaries, networks have been coupled and compared using single pressures as the interface solution (simple

boundary condition) against a pressure field as the interface solution. Comparing these two results against K_{true} with permeability as the quantity of measure, single interface (1x1, network A, constant) pressure has an error of 76% whereas pressure field solution (4x4, network A, linear) has an error of -1.7%. Clearly pressure field as the interface boundary condition, approximates the actual boundary condition of in-situ porous media.

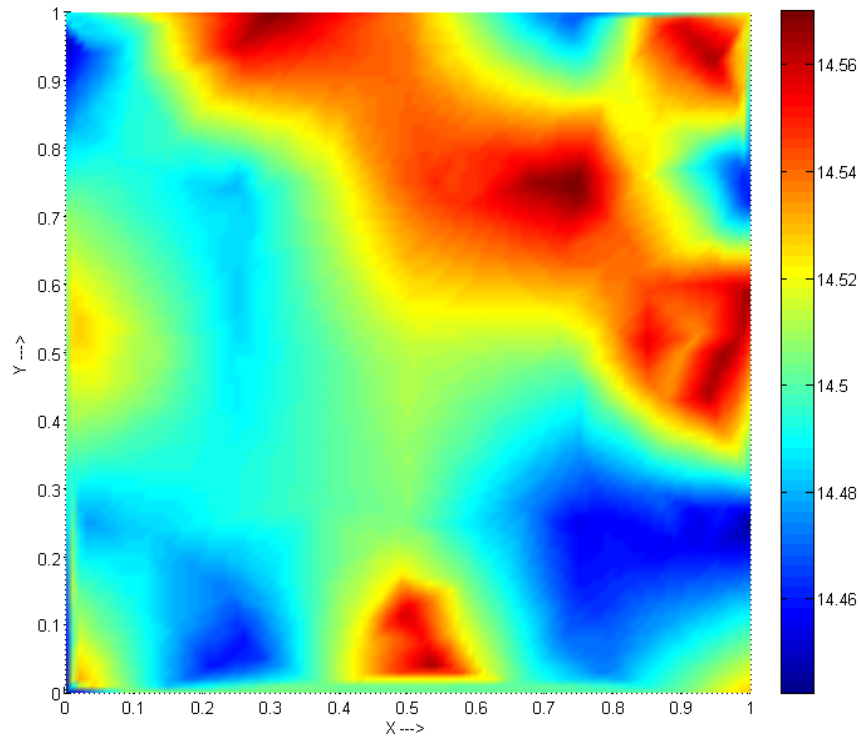


Figure 10(a):Contour plot of the true interface pressure solution

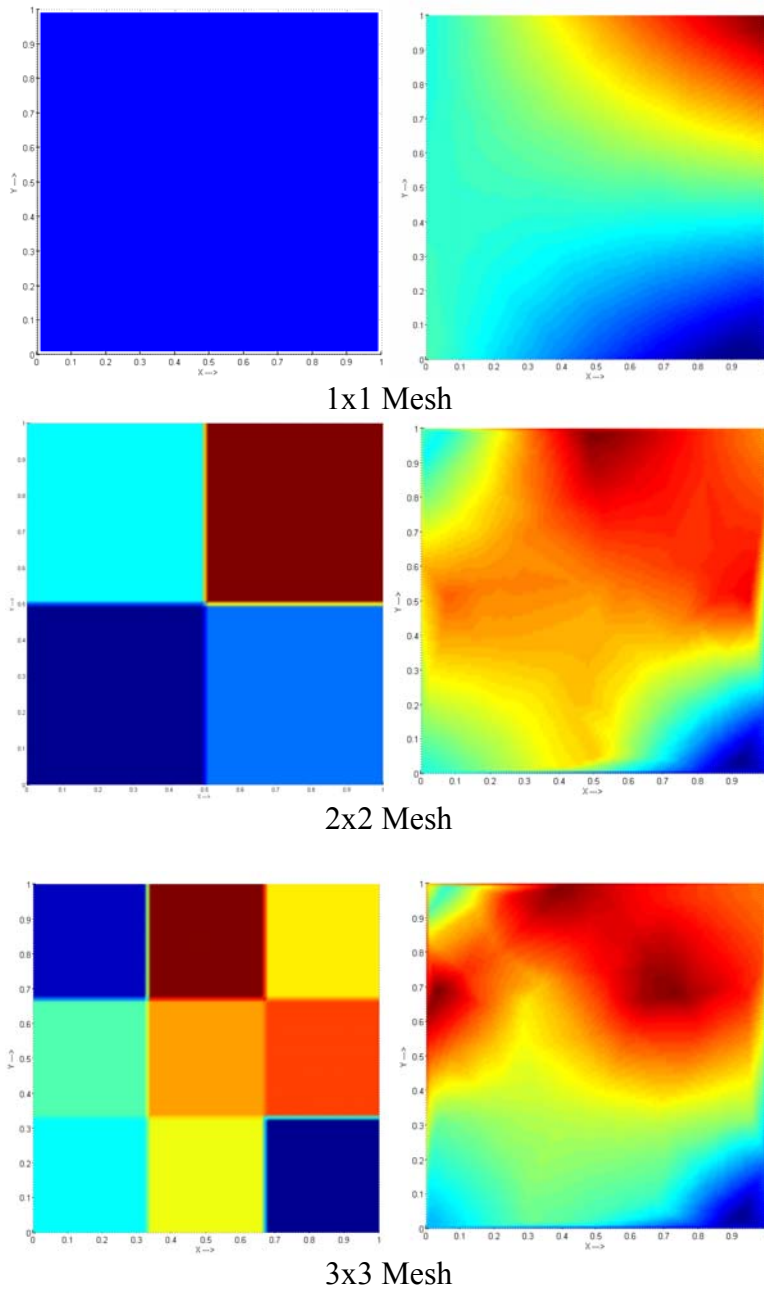


Figure 10(b): Contour Plots of the K_{mortar} solutions. Pressure solution taken from the interface between the 3(row) X 5(column) sub-network and the 3(row) X 6(column) sub-network (refer fig. 6).

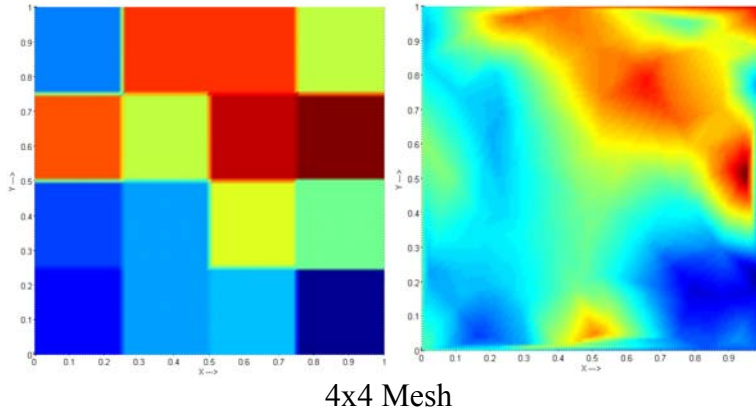


Figure 10(b): (continued) Contour Plots of the K_{mortar} solutions. Pressure solution taken from the interface between the 3(row) X 5(column) sub-network and the 3(row) X 6(column) sub-network (refer fig. 6).

Table 2: Pore network model simulation times, for 1,000,088 pores (network-A). Simulation times (K_{mortar}) can be further improved by parallel computing. Simulations have been run using one node of the 1300 node Lonestar Linux Cluster (TACC). A node consists of a Dell PowerEdge 1955 blade running a 2.6 x86_64 Linux kernel. Each node contains two Xeon Intel Duo-Core 64-bit processors on a single board, as an SMP unit. The core frequency is 2.66GHz and supports 4 floating-point operations per clock period with a peak performance of 10.6 GFLOPS/core or 42.6GFLOPS/node. Each node contains 8GB of memory

Ktrue	$K_{\text{mortar-constant}}$				$K_{\text{mortar-linear}}$			
	1x1	2x2	3x3	4x4	1x1	2x2	3x3	4x4
Time (hr)	Time (hr)	Time (hr)	Time (hr)	Time (hr)	Time (hr)	Time (hr)	Time (hr)	Time (hr)
36.12	5.70	7.99	11.82	17.29	7.70	11.19	16.10	22.41

CHAPTER 5: CONCLUSION

Pore-scale network modeling has gained steady prominence for accurate prediction and understanding of macroscopic properties in porous media. Networks are generated either by mapping directly from real media or stochastically (used here) to simulate their heterogeneous pore structure. Current pore-scale models employ artificial, unrealistic boundary conditions which affect the accuracy of the petrophysical properties of interest. Moreover, these models are often not large enough to be a representative elementary volume (REV).

Mortar coupling is a domain decomposition technique in which subdomains are coupled together through a low degree of freedom mortar space defined on a coarse grid. Here, we have shown qualitatively and quantitatively that mortars are capable of producing accurate, realistic boundary conditions on pore network models. More accurate upscaled properties (e.g. permeability) can be obtained using this approach. Accuracy can be improved using higher order basis functions (constant, linear) and finer mortar mesh size. One observation that is made is networks have optimum mesh sizes and over-meshing these networks leads to a poor solution. The mortar mesh must be coarser than the sub-domain (boundary pores on the network).

Large network models ($\sim 10^6$ pores) were decomposed into 100 sub-networks and coupled using finite element mortars. Quantitative comparison shows good agreement between the permeability of the mortar-coupled sub-networks and the larger parent network, especially for mortars with linear basis functions (a 3×3 grid gave optimal results). The sub-networks are very heterogeneous with large permeability variations (10^2) as that would be seen in actual heterogeneous rock. Coupling using a finite difference approach (where sub-network permeabilities were directly substituted into a

finite difference grid) resulted in much worse upscaled values for permeability. The mortar coupling approach outlined in this work provides a novel and accurate upscaling technique.

The coupling approach aids in maintaining the accuracy of pore-level networks with decreased computational effort (table 2). Moreover, the work provides a framework for direct substitution of pore-level models in continuum simulators. Network models can replace fine grids (e.g. near wells) and be coupled (using mortars) to adjacent pore- or continuum-scale models. Future work will focus on using the methods developed here and extend it to allow for direct implementation in continuum-scale simulators.

APPENDIX A

Table A.1: Network generation parameters (Refer eq. 1) Both network types (A and B) have the same parameter range. Network B is anisotropic than network A due to the distribution of high & low permeability networks into channels having high and low flow-regimes.

	Network A				Network B			
	<i>a</i>	<i>b</i>	<i>c</i>	Pores	<i>a</i>	<i>b</i>	<i>c</i>	Pores
1	2.6	170	60.5	9041	3.9	162	51.5	14641
2	2.4	233	19.6	3828	3.3	186	38.7	12870
3	2.1	253	14.1	9093	3.4	245	40.7	6867
4	3.5	260	50.4	14969	3.1	190	69.5	12884
5	2.1	140	65.4	17428	2.1	192	62.7	15722
6	2.8	195	22.4	11331	3.2	199	36.0	8106
7	2.6	210	60.1	16218	3.0	173	61.7	14747
8	2.7	218	31.2	2372	3.3	139	51.1	7018
9	2.8	92	21.2	12895	2.8	256	55.5	13565
10	2.2	185	66.2	10646	3.1	196	38.5	18000
11	2.9	265	66.4	5594	3.2	231	62.9	15874
12	2.8	126	29.3	11142	2.4	234	63.6	9217
13	4.0	206	51.6	5572	3.4	202	28.9	14483
14	2.1	238	58.5	3299	3.8	128	54.0	2614
15	2.3	158	28.0	8966	2.8	257	66.6	12583
16	3.0	259	62.6	7161	2.9	146	49.0	17824
17	3.7	89	59.1	7736	2.1	273	44.1	2000
18	2.0	243	56.4	14696	3.8	138	68.0	15095
19	3.9	112	24.7	2473	2.8	173	38.2	6420
20	3.8	203	68.6	15455	3.0	256	45.2	2160
21	2.1	248	22.9	15636	3.4	261	50.6	12931
22	2.4	143	32.2	10691	3.6	143	11.4	14575
23	2.7	144	23.6	7623	2.9	287	27.9	12446
24	3.5	123	44.5	13611	3.9	251	42.2	17892
25	3.3	281	41.3	5238	2.2	210	19.9	3700

	Network A				Network B			
	<i>a</i>	<i>b</i>	<i>c</i>	Pores	<i>a</i>	<i>b</i>	<i>c</i>	Pores
26	3.2	152	31.5	10519	3.0	122	35.6	17164
27	2.7	158	20.0	4732	3.3	201	18.5	16000
28	3.1	124	38.0	17584	2.7	152	14.0	16932
29	2.9	100	16.3	15672	2.1	253	40.8	12692
30	3.4	284	37.0	4931	3.1	259	12.5	15411
31	2.1	214	50.5	14109	3.4	271	48.2	14790
32	2.6	232	39.1	4841	2.7	100	50.2	2800
33	3.8	173	18.0	9135	3.2	181	14.6	5687
34	3.9	184	67.7	4263	3.2	201	12.2	2090
35	2.3	198	55.3	7929	2.1	261	41.3	15682
36	3.5	93	37.6	13634	2.2	158	36.2	9627
37	2.1	212	23.2	14157	2.9	115	13.4	16661
38	4.0	177	49.2	13681	2.6	186	20.6	2112
39	3.1	189	46.5	12315	2.6	147	13.4	14701
40	3.5	107	64.3	17211	2.3	155	61.1	6131
41	2.7	105	54.8	17840	3.1	258	25.6	15143
42	3.6	245	17.1	8234	4.0	94	64.5	15044
43	3.0	141	64.3	2033	3.7	254	51.6	13529
44	2.2	157	42.2	7811	3.8	126	63.6	15321
45	3.8	216	55.9	12886	3.5	247	55.3	10965
46	2.0	271	13.4	17097	2.8	197	22.2	2034
47	2.3	256	62.6	8641	3.2	91	28.7	12419
48	3.8	286	36.3	16375	3.7	152	53.8	2877
49	2.1	94	34.3	10207	3.9	275	40.1	12566
50	3.6	90	56.7	15168	3.5	231	23.2	2095
51	2.4	157	58.4	10749	2.0	133	40.1	15409
52	3.5	208	24.8	8499	2.3	217	54.7	14000
53	2.6	128	22.7	8385	3.2	203	54.5	2167
54	3.5	107	66.4	4440	2.4	230	48.2	2235
55	2.2	91	31.7	11193	3.4	214	16.2	16596
56	2.9	116	22.1	3720	2.3	129	58.3	13931
57	4.0	283	44.5	11131	3.2	258	18.4	12654
58	2.1	285	14.5	9354	2.6	275	61.4	14136
59	3.8	282	35.4	15311	2.4	132	53.3	15573

	Network A				Network B			
	<i>a</i>	<i>b</i>	<i>c</i>	Pores	<i>a</i>	<i>b</i>	<i>c</i>	Pores
60	3.5	219	67.1	13522	3.7	96	56.6	14576
61	2.8	125	25.0	7372	3.8	278	68.8	18000
62	3.4	102	55.1	13291	3.4	188	55.3	14708
63	2.8	223	57.0	16504	3.5	89	26.9	14616
64	3.4	126	68.7	10373	3.9	288	64.8	11230
65	2.4	183	39.0	2496	2.5	279	62.2	11222
66	3.6	168	29.9	17837	2.3	289	58.4	2000
67	3.7	240	45.6	15613	2.1	270	67.9	10137
68	2.9	197	65.9	3250	2.1	246	45.7	7078
69	4.0	103	21.9	5053	3.7	167	26.3	15850
70	3.2	158	66.8	12788	3.1	258	27.1	4292
71	2.8	255	55.7	13752	3.6	242	38.4	14892
72	3.7	203	36.4	14417	3.5	113	17.2	2138
73	2.0	185	50.2	16820	2.1	282	51.7	16067
74	2.7	287	35.8	16190	2.6	287	24.5	2999
75	2.3	105	66.6	11401	3.7	184	31.5	3100
76	3.1	130	35.8	12893	3.2	155	38.7	8680
77	3.4	107	37.2	9984	3.6	192	24.0	2120
78	2.2	96	29.6	10650	3.7	248	31.9	16679
79	3.0	111	68.8	14969	2.8	144	56.2	2190
80	3.0	166	53.7	11547	3.2	256	24.2	13898
81	3.4	138	26.9	15297	2.5	218	62.5	10616
82	2.7	183	56.3	13796	2.7	260	51.2	12275
83	2.2	123	53.8	11045	2.6	259	19.6	13520
84	2.7	103	28.1	8779	2.8	154	69.7	6243
85	3.3	109	62.6	3616	2.0	264	68.1	13400
86	3.1	174	29.4	10217	2.0	187	55.3	8125
87	3.0	186	46.9	5048	3.2	153	66.2	13366
88	2.8	171	33.0	16293	2.9	278	44.0	6280
89	3.7	247	16.3	11744	3.4	287	44.3	12676
90	3.8	278	62.5	4740	2.3	210	63.7	3397
91	4.0	269	50.9	10567	3.8	205	20.2	3360
92	3.1	267	16.2	5392	3.6	95	65.4	2601
93	3.5	123	21.2	5564	2.4	252	30.9	3589

	Network A				Network B			
	<i>a</i>	<i>b</i>	<i>c</i>	Pores	<i>a</i>	<i>b</i>	<i>c</i>	Pores
94	3.5	153	38.4	9677	2.9	143	39.7	2779
95	3.8	266	45.5	11552	2.9	195	19.5	3207
96	3.3	125	55.7	11990	3.1	195	17.2	3904
97	2.5	268	40.9	3187	3.2	216	62.2	2700
98	3.4	266	20.8	9200	3.6	168	37.5	2964
99	2.5	167	27.0	12632	2.9	281	18.9	3320
100	2.0	220	68.6	2750	2.8	221	23.2	3869

GLOSSARY

C	= Coordination number, dimensionless
L	= Throat length, m
R	= Throat radius, m
a, b, c	= Probability parameters, dimensionless
$p(x)$	= Probability distribution, dimensionless
$F(x_1)$	= Cumulative probability distribution, dimensionless
rnd1, x1	= Sample parameters, dimensionless
Q	= Flow, m^3/s
q_L, q_R	= Flow in the left and right networks comprising the interface, m^3/s
ΔP	= Pressure drop, N/m^2
∂P	= Incremental pressure increase, N/m^2
μ	= Viscosity, $N\cdot m/s$
r	= Throat radius, m
X, x	= X-axis
Y, y	= Y-axis
K, k	= Permeability, Darcy
A	= Model area, m^2
L_{model}	= Model length, m
i	= Boundary pore, dimensionless
j	= Interior pore, dimensionless
P_a, P_b	= Inlet and Outlet Pressure, N/m^2
F	= Net flux, m^3/s

m	= Mortar coarse grid, dimensionless
$sd1, sd2$	= Sub-domains 1 and 2, dimensionless
N	= Size of Jacobian system, dimensionless
P	= Pressure, N/m^2
α	= Basis function coefficients, dimensionless
φ	= Basis function, dimensionless
g	= Throat conductivity
V	= Velocity, m/s
ρ	= Density, kg/m^3
\vec{g}	= Gravity term
Φ	= Flow Potential

REFERENCES

- Arbogast T., Cowsar L. C., Wheeler M. F., and Yotov I., Mixed finite element methods on non-matching multi-block grids, *SIAM J. Numerical Analysis.*, 37 (2000), pp. 1295–1315
- Arbogast T., Pencheva G., Wheeler M.F., Yotov I., A multiscale mortar mixed finite element method. *SIAM Multiscale J.* 6(1):319–346 (2007)
- Arns C.H., Knackstedt, Pinczewski MA, Lindquist WV, Accurate estimation of transport properties from microtomographic images, *Geophysical research letters*, Vol. 28 2001, pp. 3361-3364
- Bakke S., Oren P.E.: 3-D pore-scale modeling of sandstones and flow simulations in the pore networks. *SPE J.* 2(2), 136-149 (1997)
- Balhoff M.T., Karsten E. Thompson and Martin H, 2006, Coupling pore-scale networks to continuum-scale models of porous media, *Computers and Geosciences*, Volume 33 , Issue 3 (March 2007) Pages 393-410
- Balhoff M.T., Sunil G. T., Wheeler M.F., January 2007, Mortar coupling and upscaling of pore-scale models, DOI 10.1007/s10596-007-9058-6
- Bernardi C., Maday Y., and Patera A. T., *A new nonconforming approach to domain decomposition*, 1994
- Blunt M. and Peter K, March 1990. Macroscopic parameters from simulations of pore-scale flow, BP research centre
- Bryant S.L., and Blunt M, 1991, Prediction of Relative Permeability in simple porous media BP research centre.
- Bryant S.L., King P.R., and Mellor D.W. 1993a, Network Model Evaluation of permeability and spatial correlation in a real random sphere packing *Transport in Porous Media* 11 (1): 53–70. doi:10.1007/ BF00614635.
- Bryant S.L., Mellor D.W., and Cade C.A. 1993b, Physically representative network models of transport in porous media *AIChE Journal* 39 (3): 387–396. doi:10.1002/aic.690390303.
- Chen J D and David W., Colloid J, *Interface Science Pore-Scale Viscous Fingering in Porous Media*, 108, 304 (1985)
- Darryl H. F, and Martin J. B, SPE, Stanford U., *Network Modeling of Three-Phase Flow in Porous Media*, SPE 3881-PA, 1998

- Dowd B.A., Andrews A.B., Marr R.B., Siddons D.P., Jones K.W., and Peskins A.M., 1992, Advances in x-ray computed microtomography at the nsls, *Advances in X-ray Analysis*, 42
- Fatt I., U. of Southern California, 1956, The Network Model of Porous Media, *Petroleum Transactions, AIME*, Volume 207, 1956, pages 144-181, 574-G
- Glowinski R. and Wheeler M. F., Domain decomposition and mixed finite element methods for elliptic problems, SIAM, Philadelphia, 1988, pp. 144–172.
- Grader A.S. and O’Meara D.J. Jr.: “Dynamic Displacement Measurements of Three-Phase Relative Permeability’s Using Three Immiscible Liquids,” SPE 18293, 1988
- Haines W.B., 1930. Studies in the physical properties of soil, *Journal of Agriculture Science*, 20:97
- Koplik J. and Lasseter T.J., *Chemical Engineering Communications* 26, 285 (1984)
- Leormand R. and Zarcone C., *Transport in Porous Media* 4, 599, Capillary fingering: Percolation and fractal dimension (1989).
- Lin C. and Cohen M.H., 1982, Quantitative methods for microgeometric modeling, *Journal of Applied Physics*, 53:4152 4165
- Lymberopoulos D.P. and Payatakes A.C., Derivation of geometrical and correlation properties of porous media from pore chart analysis of serial section data, *J. Colloidal Interface Sci.*, 150(1):61 80
- Małgorzata P, Wheeler M. F. and Yotov Ivan, (2001) Mortar upscaling for multiphase flow in porous media, *Computational Geosciences* 6: 73–100, 2002.
- Melrose, J.C., 1965. Wettability as related to capillary action in porous media, *Journal of Petroleum Science and Engineering*, 5(3): 259-271.
- Payatakes A.C., *Annual Review of Fluid Mechanics* 14, 365, Dynamics of Oil Ganglia during Immiscible Displacement in Water-Wet Porous Media (1982)
- Philippe M. D., 1988, Permeability, conductivity and pore geometry of sandstone *Journal of Geophysical Research* 93(B7):7729 7740
- Piri M. and Martin J. B. (2005) Three dimensional mixed wet random pore-scale network modeling of two and three phase flow in porous media. DOI: 10.1103/PhysRevE.71.026302

Robert M S, Mark A K, Adrian P. S, Pinczewski W.V., Lindquist WB, Venkatarangan A. and Lincoln P., 2002, Direct and stochastic generation of network models from tomographic images; effects of topology on two phase flow properties, Transport in Porous Media, Volume 46, Numbers 2-3, February 2002 , pp. 345-371(27)

Sarkar M.R.H. and Siddiqi S., 2009, Advances in Micro-CT based evaluation of reservoir rock, SPE-126039

Venkatarangan AB, 2000, Geometric and statistical analysis of porous media, State University of New-York at Stony Brook